



OPEN ACCESS

EDITED BY

Hans Uwe Dahms,
Kaohsiung Medical University, Taiwan

REVIEWED BY

Fajin Chen,
Guangdong Ocean University, China
Bo-Shian Wang,
National Academy of Marine Research
(NAMR), Taiwan

*CORRESPONDENCE

Jun Du

✉ dujun@fio.org.cn

Dongqi Gu

✉ friendgu@fio.org.cn

RECEIVED 27 July 2023

ACCEPTED 03 January 2024

PUBLISHED 29 January 2024

CITATION

Yan W, Du J, Gu D, Wang Y, Xu G, Wang G, Sun Y, Li P and Chen W (2024) Composition and concentration of suspended matter in the Zhongsha Great Atoll, South China Sea, before and during the summer monsoon. *Front. Mar. Sci.* 11:1268294. doi: 10.3389/fmars.2024.1268294

COPYRIGHT

© 2024 Yan, Du, Gu, Wang, Xu, Wang, Sun, Li and Chen. This is an open-access article distributed under the terms of the [Creative Commons Attribution License \(CC BY\)](https://creativecommons.org/licenses/by/4.0/). The use, distribution or reproduction in other forums is permitted, provided the original author(s) and the copyright owner(s) are credited and that the original publication in this journal is cited, in accordance with accepted academic practice. No use, distribution or reproduction is permitted which does not comply with these terms.

Composition and concentration of suspended matter in the Zhongsha Great Atoll, South China Sea, before and during the summer monsoon

Wenwen Yan^{1,2}, Jun Du^{1*}, Dongqi Gu^{1*}, Yongzhi Wang¹, Guoqiang Xu^{1,2}, Guanxun Wang^{1,3}, Yonggen Sun¹, Ping Li¹ and Wei Chen⁴

¹Key Laboratory of Coastal Science and Integrated Management, First Institute of Oceanography, Ministry of Natural Resources, Qingdao, Shandong, China, ²Key Laboratory of Marine Environment and Ecology, Ministry of Education, Ocean University of China, Qingdao, Shandong, China, ³College of Oceanic and Atmospheric Sciences, Ocean University of China, Qingdao, Shandong, China, ⁴Qingdao Geological Exploration Institute, China Metallurgical Geology Bureau, Qingdao, Shandong, China

Suspended matter in seawater carries abundant nutrients and carbon, playing a significant role in carbon cycle and ecosystem in many oceanic settings such as atolls. The Zhongsha Great Atoll (hereafter ZGA), located in the deep South China Sea, sustains a both regionally and globally important ecosystem. Characteristic of the suspended matter in this area, however, remains poorly investigated. Using a data set encompassing temperature, salinity, depth, and suspended matter concentration (hereafter SMC) of seawater collected respectively in May 2019 (spring-summer monsoon transition period) and June 2020 (summer monsoon outbreak period) in the ZGA, the main components and spatial distribution of suspended matter together with their influencing factors were comprehensively analyzed. Our results show that the components of suspended matter vary widely in space and include more than 20 types of materials such as planktonic remains and biogenic siliceous debris. During the transit between spring and summer monsoons, the SMC in seawater was generally low, with an average value of approximately 3.26 mg L⁻¹, which decreased from the surface to the middle layer and then increased to deep waters; Horizontally, the SMC in the west was generally higher than that in the east likely because the wind-driven current transport significant amounts of particles from the east to the west. During the 2020 summer monsoon outbreak, average SMC in this area was 6.27 mg L⁻¹, higher than that during the 2019 spring-summer monsoon transit. Moreover, significantly higher SMC in the 1-100 m layer and lower SMC in the 150 m layer were observed in the west. Owing to the impact of mesoscale eddies, low SMC in the surface layer and high concentrations in the bottom layer can occur in parts of the ZGA, leading to the deepening of the west-high and east-low distribution layers of SMC during the 2020 summer monsoon outbreak. Notably, we for the first time have observed an anomalously high SMC in the 1–100 m layer of the northwest area during the 2020 summer monsoon outbreak. This anomaly is higher than any previously reported values in the South China Sea and can be attributed to the multiple monsoon impacts. Sources of suspended

matter, topography, currents, and wind field were identified as the main factors influencing the spatial distribution of SMC in this area. Our findings provide a basic context for understanding the sources and dynamics of suspended material in atolls.

KEYWORDS

Zhongsha Great Atoll, suspended matter, summer monsoon, material transport, ocean current

1 Introduction

Suspended matter is all particulate matter present in water in a suspended state and can be divided into two main categories: combustible components (biogenic particles and various flocs) and non-combustible components (sand and mud particles, rock, and mineral fragments) (Bubnova et al., 2020; Chong et al., 2011; Wang, 2014). Suspended matter of terrestrial origin is the main source of the widely distributed muddy deposits in estuaries and shelves (Milliman and Syvitski, 1992). These terrestrial suspended matters contain abundant organic carbon, thus playing a vital role in the global carbon cycle. Besides, suspended matter adsorbs large amounts of nutrient, indirectly influencing primary productivity in seawater by promoting phytoplankton blooms. The transport of suspended matter and its sorptive nutrient thus affect marine ecosystems (Wang H. et al., 2022). Therefore, the components, concentration, and transport-deposition processes of suspended matter exert tremendous controls on global carbon cycle and climate change (Manik and Firdaus, 2021).

The ZGA is located in the deep region of the South China Sea, as shown in Figure 1A. Impacted by multiple interacting flow systems and water masses, the hydrodynamic setting in the atoll is extraordinarily complex, making it difficult to explore the space-time variations of suspended matter in the upper water column (Guo et al., 2005; Huang H. et al., 2020; Liu et al., 2022). To date, most previous studies on this area have focused on sedimentology and tectonic geology (Huang H. et al., 2020; Zhang et al., 2022). However, the suspended matter in the upper water column of this area has not been investigated so far. A systematic study on space-time variations of suspended matter in the upper water column will be of considerable scientific importance for understanding modern sedimentation processes and the oceanic carbon cycle (Nittrouer et al., 2021).

In this study, we aimed to study the spatial distribution of suspended concentration in the ZGA during the spring-summer monsoon transition period and summer monsoon outbreak period based on field measurement data, combined with the temperature and salt distribution characteristics, and to provide a preliminary discussion on the influencing factors that reflect the characteristics of modern sedimentation in the ZGA.

2 Materials and methods

2.1 Study area

The Zhongsha archipelago, mainly including ZGA and Huangyan Island, extend from the Constitutional Dark Sands (16° 20'N, 116°44'E) in the north to the Central South Dark Sands (13°57' N, 115°24'E) in the south, from Huangyan Island (15°08'N, 117°45' E) in the east to the floodplain of the Zhongsha Atoll (15°38'N, 113° 43'E) in the west. This archipelago, together with the Dongsha, Xisha, and Nansha archipelagos, constitute the major islands in the South China Sea (Huang X et al., 2020; Wang et al., 2022). The Zhongsha archipelago, is located on a faulted continental slope at a water depth of ~2000 m in the South China Sea, surrounded by prominent fracture troughs including the central deep basin at a water depth of >4000 m to the east and the Zhongsha Trough at a water depth of 2000 m to the west. The ZGA is located in the center of the Zhongsha archipelago, with its reef body submerged below the sea surface (Huang H et al., 2020; Quanshu et al., 2007).

2.2 Data and methods

2.2.1 Sampling and data collection

Using a marine survey vessel “Yue Xia Fishing Finger 1020”, two cruises were performed respectively from May 11 to May 29, 2019, and from June 20 to July 6, 2020, to investigate the suspended matter in the ZGA. 41 stations and 34 stations inside and surrounding the ZGA were respectively sampled and surveyed using a SBE 911plus CTD (conductivity, temperature and depth) system during the 2019 and 2020 voyages, as shown in Figure 1B. Most stations were surveyed and sampled for six water layers at water depths of 1, 25, 50, 75, 100, and 150 m. For some stations in shallower area, only three layers of water were investigated at water depths of 1 m (surface layer), 25 m, and 50 m. Besides, the CTD recorded the information of depth, temperature, and salinity of each water layer during the water sample collection.

During the investigation in May 2019, winds below grade 4 in the ZGA were observed to shift their directions from northeasterly

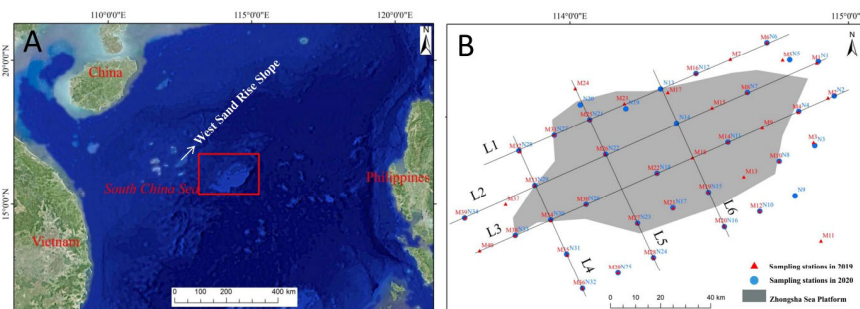


FIGURE 1 Study area. (A) Schematic diagram of the location of the study area (B) Sampling stations during the investigations in 2019 and 2020.

and easterly winds (spring monsoon) to southwesterly or southerly winds (summer monsoon), demonstrating a clear transition between spring and summer monsoons (Wang Y. Z et al., 2022). In comparison, stronger southwesterly winds (grade 4 and above) dominated the ZGA area during the cruise in June 2020, indicating the outbreak of the summer monsoon.

2.2.2 Sample processing

Generally 2000 mL or 1200 mL (at some individual layers) of seawater were collected and filtered with Millipore acetate membranes (47 mm in diameter and 0.45 μm in pore size). Before the filtration, the membranes were weighed to constant weight using a one-hundred-thousandth part of an electronic balance. In this study, one blank correction membrane was used during the filtration of seawater sample at each station to get a correction value. First, we used a stainless-steel tweezers to place a pre-weighed membrane on top of a pre-weighed and labeled blank correction membrane, and place them together into the filter; after shaking the seawater sample sufficiently, pour it into a measuring cylinder and measure 2000 ml; start the vacuum pump and pour the water sample into the filter. For desalination purpose, we rinsed the membrane three times with 50 ml of distilled water after filtration, and then drain again. Use stainless steel tweezers to remove the filter membrane and place it in the original filter membrane box. Dry it under infrared lamp at low temperature (50°C) or air dry in a natural environment. Close the filter membrane box, save it in order, and conduct filter membrane blank correction and sample determination in the laboratory simultaneously to ensure the accuracy of the results. The suspended matter concentration (mg/L) in each water sample was calculated as Equation 1:

$$SMP = \frac{M_p - M_s - \Delta M}{V} \quad (1)$$

where M_p is the mass of post-filtration filter membrane (mg), M_s is mass of the pre-filtration filter membrane (mg), ΔM is the correction value of blank filter membrane (mg), and V is the volume of filtered water sample (L).

2.2.3 Components of suspended matter

We cut a piece of filter membrane sized $\sim 3 \text{ mm} \times 5 \text{ mm}$ from the center of the dried filter membrane. The cut membrane was

scanned with a Scanning electron microscopy (SEM Quanta 200) to look at the components, shapes, and structures of suspended matters. The scanning electron microscope was operated in high-vacuum mode with a working distance of 10 mm, a beam spot of 5, and an acceleration voltage of 25 kV. T. We used an X-ray energy spectrum analyzer (GENESIS 2000) to further identify the chemical features of the suspended matter.

3 Results

3.1 Temperature and salinity of seawater

During the transition of spring-summer monsoons (May 2019), the temperature of surface (1m layer) seawater in the southwest of ZGA was than the northeast. This spatial distribution of temperature is generally opposite to that of the 25-m layer where similarly higher temperature in the southwest and lower temperature in the northeast was observed. In comparison to the 25 m layer, the 50-m layer has a similar but slightly different spatial distribution of seawater temperature, with larger areas of low temperature and greater high-low temperature difference (up to 6°C). The seawater temperature at 75-m layer showed a clear horizontal distribution pattern of lower temperature in the southwest and higher temperature in other areas. At 100-m water depth, higher temperatures were observed in the center of the ZGA. However, the average seawater temperature at the 150-m layer was 5.05°C lower than that of the 100-m layer, indicating an average temperature decrease amplitude of approximately 0.08°C m^{-1} . Over both vertical and horizontal scales, the range of the low-value zone increased significantly with water depth. As to the salinity of seawater, the spatial distribution at each layer (depth) was similar to that of the water temperature in the surface (1 m) water layer, showing a general decreasing trend from southwest to northeast. Vertically, the seawater salinity generally increased with water depth.

During the outbreak of summer monsoon (June 2020), seawater temperature at the surface layer was higher than 30°C with relatively lower values observed in the southwest than the northeast. There were two high surface water temperature areas in the northeast and northwest and a low-temperature area in the

southwest. Water temperature at 25-m layer were relatively higher in the middle and north than the southwest. The spatial distribution of seawater temperature at the 50-m layer significantly differed from that at the 25-m layer, with two low-temperature zones located in the west and south, and two high-temperature zones in the northwest and northeast. The spatial distribution of seawater temperature at the 75-m layer varied greatly. The 100 m and 150 m layers had similar spatial distribution pattern of water temperature as the surface water, with higher values observed in the central west and northeast. As to the seawater salinity, the surface layer had a low value in the middle east of the study area (33.90–34.00). The seawater salinities at the 25 m and 50 m layers were opposite to the temperature variation, and the low-value area gradually expanded from the northeast to the southwest with increasing water depth. Horizontally, the salinity of the 75 m layer increased gradually from southwest to northeast. The salinity distribution in the 100–150 m layers was similar to the temperature distribution, and high-temperature concurred with low-salinity in both the west-central and northeast areas.

3.2 Components of suspended matter

After preliminary selection for the results of SEM and energy spectrum analysis, the component and quantity of suspended matter in the ZGT were most abundant at the 25-m layer; therefore, the larger particle profiles of some representative components in this layer were selected for a detailed representation in this study. According to previous studies (Chen et al., 1998; Guo et al., 2001; Sun et al., 2018), the suspension fractions in the study area were classified into five types according to their origin and sources: biogenic debris, terrigenous debris, authigenic mineral particles, organic films, and modern artificial material, which can be further subdivided into over 20 sub-types. Our SEM results show that different stations have different components of suspended matter, as listed in Table 1. At Station N30 and N16, the suspended matters are dominated by terrigenous debris, which constitutes 58.8% of the total content. On contrast, Station N16 showed a higher biogenic debris content of 30% than a 23% at Station N30. At Station N5, terrigenous debris and authigenic minerals account for 40.7% and 37% respectively, followed by a lower content of biogenic components (7.4%). Biogenic debris accounted for 45% of the suspended matter at Station N32, which is the highest among all stations. The proportion of modern anthropogenic material ranged from 0% to 6%. The organic film was only observed at Station 200.

3.2.1 Biogenic debris

3.2.1.1 Phytoplankton remains and fragments

The biogenic debris was dominated by phytoplankton remains and fragments, among which diatoms (SiO₂·nH₂O) were most abundant in number and species. Most of these diatoms have intact remains and particle size of 15–100 μm (Figures 2A–F). The zooplankton remains were dominated by radiolarian shells (SiO₂·nH₂O), with abundant species and particle size of 25–75 μm (Figure 3).

TABLE 1 Components of suspended matter at selected stations.

| Station NO. | Total number of components | Biogenic debris | Percentage (%) | Terrigenous debris | Percentage (%) | Authigenic debris | Percentage (%) | Organic films | Percentage (%) | Mordern artificial materials | Percentage (%) |
|-------------|----------------------------|-----------------|----------------|--------------------|----------------|-------------------|----------------|---------------|----------------|------------------------------|----------------|
| N30 | 17.0 | 4.0 | 23.5 | 10.0 | 58.8 | 2.0 | 11.8 | 0.0 | 0.0 | 1.0 | 5.9 |
| N22 | 10.0 | 5.0 | 50.0 | 1.0 | 10.0 | 4.0 | 40.0 | 0.0 | 0.0 | 0.0 | 0.0 |
| N16 | 17.0 | 5.0 | 29.4 | 10.0 | 58.8 | 1.0 | 5.9 | 0.0 | 0.0 | 1.0 | 5.9 |
| N5 | 27.0 | 2.0 | 7.4 | 11.0 | 40.7 | 10.0 | 37.0 | 1.0 | 3.7 | 1.0 | 3.7 |
| N32 | 20.0 | 9.0 | 45.0 | 7.0 | 35.0 | 4.0 | 20.0 | 0.0 | 0.0 | 0.0 | 0.0 |
| Total | 127.0 | 39.0 | 30.7 | 48.0 | 37.8 | 30.0 | 23.6 | 1.0 | 0.8 | 7.0 | 5.5 |

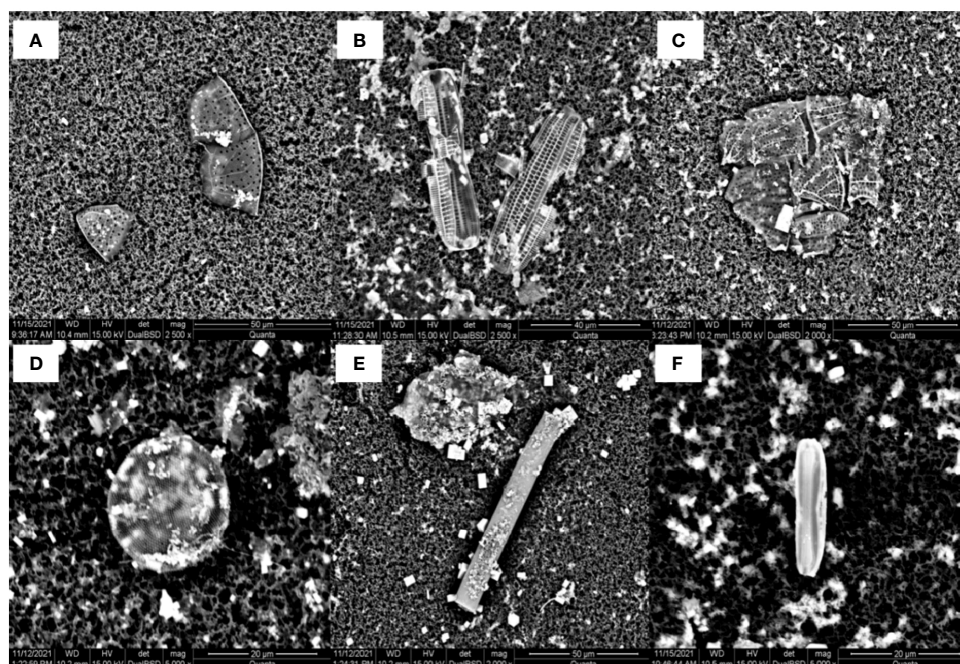


FIGURE 2

Planktonic remains and fragments. (A–C) Fragments of different diatom species from stations N30, N32, and N22, respectively. (D–F) More complete diatom remains of different species from stations N10, N32, and N32, respectively.

3.2.1.2 Biogenic carbonate fragments

The biogenic carbonate debris is rich in shape types, mostly in the form of single crystal. Biogenic carbonate is mainly composed of calcium magnesium carbonate and magnesium carbonate; some of the identifiable minerals are dolomite [$\text{CaMg}(\text{CO}_3)_2$], calcite (CaCO_3), and magnesite [$\text{Mg}(\text{CO}_3)$]. The particle size of the fragments varied widely from $<3\ \mu\text{m}$ to $40\ \mu\text{m}$, with dolomite having a better crystal shape and larger particle size than the others (Supplementary Figure 1).

3.2.1.3 Biogenic siliceous debris and plant fibers

The biogenic siliceous debris is biomorphic but less abundant, including sponge bone needles (Supplementary Figure 2A) with a length $>40\ \mu\text{m}$. Plant fibers are curved and elongated with curled edges, $2\text{--}7\ \mu\text{m}$ wide and $>50\ \mu\text{m}$ long, probably derived from terrestrial or aquatic plants (Supplementary Figure 2B).

3.2.2 Terrestrial debris

3.2.2.1 Lithogenous minerals

Terrigenous debris is dominated by aluminosilicate minerals including quartz, feldspar, hornblende, mica, and chlorite (Supplementary Figure 3), with a particle size of $5\text{--}40\ \mu\text{m}$.

3.2.2.2 Accessory minerals

Accessory minerals are diverse, including rutile, scheelite, and corundum (Supplementary Figure 4), with the particle size in a range of $1\text{--}50\ \mu\text{m}$.

3.2.3 Authigenic mineral

Authigenic mineral grains were dominated by particulate iron oxide aggregates, including small-grained barite. Particulate iron oxide aggregate has $10\text{--}15\ \mu\text{m}$ size and medium iron content, probably consisting of multiple small ($<1\ \mu\text{m}$) hematite-magnetite-type particles with spherical-irregular morphology (Supplementary Figure 5).

3.2.4 Organic film

The organic envelope is composed of an organic colloid, which appears as a dark paste in the electron micrograph and is often covered with multiple particles, forming an organic envelope agglomeration (Supplementary Figure 6) with a rounded irregular morphology.

3.2.5 Modern artificial materials

Artifact fragments mainly include metal scraps with a particle size of $2\text{--}30\ \mu\text{m}$. Among these, iron flakes were predominant (Supplementary Figure 7), and the particles of the alloy steel contained tungsten, manganese, nickel, and chromium but with smaller particle sizes (Supplementary Figure 7). Most alloy steels had an apparent oxygen content, likely due to partial rusting.

3.3 Spatial distribution of suspended matter concentration

During the transition of spring-summer monsoon (May 2019), a highest SMC value of $13\ \text{mgL}^{-1}$ in the study area was found at the

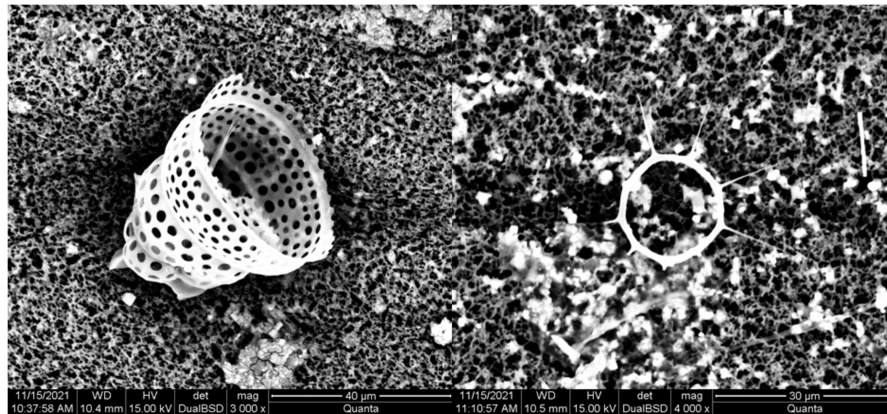


FIGURE 3
Radiolarian debris, N32.

1-m water layer at station M6 in the northeast; the lowest value of 0.25 mgL^{-1} occurred at the 75-m layer at station M37 in the southwest (Figure 4). The SMC peaked in the surface layer (1 m), decreased at 25 m water depth, and increased again at 25 m and 50 m water layers. Below 50 m, the SMC decreased with the water depths. Horizontally, the SMC in the surface layer (1 m) was higher in the northeast than in the southeast, with a variation range of $0.95\text{--}13 \text{ mgL}^{-1}$. At the 25-m layer, the SMC decreased from west to east, with a variation range of $0.95\text{--}6.3 \text{ mgL}^{-1}$. The SMC at 50-m layer was high in the northeast and low in the southwest, ranging from 0.55 mgL^{-1} to 10 mgL^{-1} . The SMC at 75-m layer was similar as

that at the 50-m layer, with a variation range of $0.25\text{--}6.3 \text{ mgL}^{-1}$. The SMC at 100-m and 150-m layers gradually decreased from west to east.

During the outbreak of summer monsoon (June 2020), the SMC in the study area was in a range of $3.05\text{--}14.65 \text{ mgL}^{-1}$. The highest and the lowest values occurred respectively in the surface layer and in the 150-m layer (Figure 5). At 25-m and 50-m layers, the SMCs were only slightly lower than that in the surface layer. From 50-m to 150-m, the SMC gradually decreased. Over a horizontal scale, the SMC values in the surface layer (1 m) were lower in the middle than other areas, with the overall SMC in the west higher than that in the

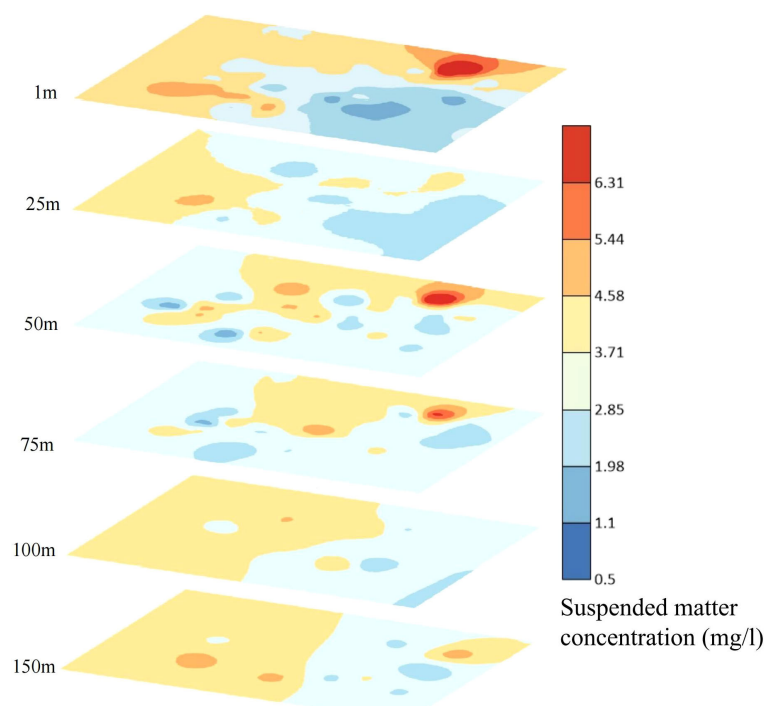


FIGURE 4
Spatial distribution of suspended matter concentration during May 2019.

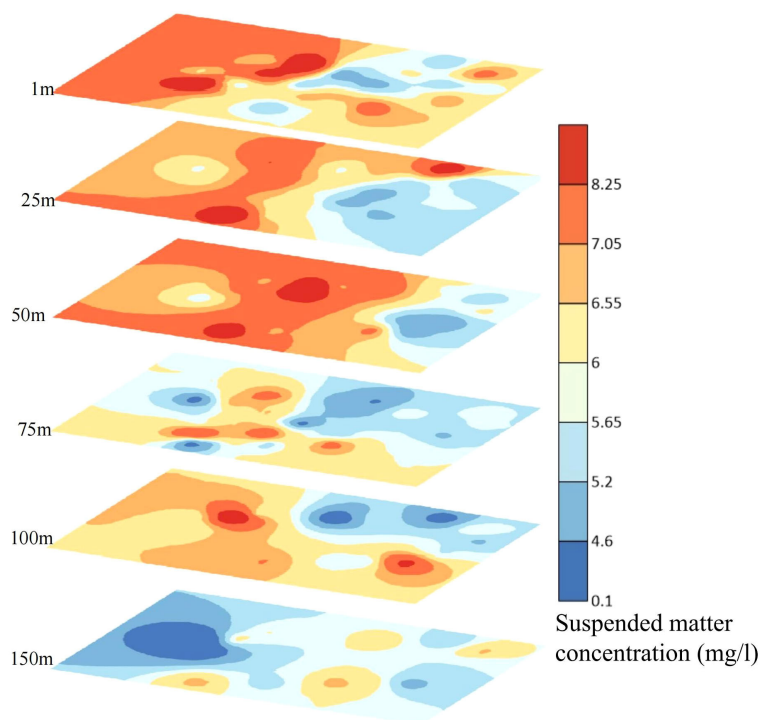


FIGURE 5
Spatial distribution of suspended matter concentration during June 2020.

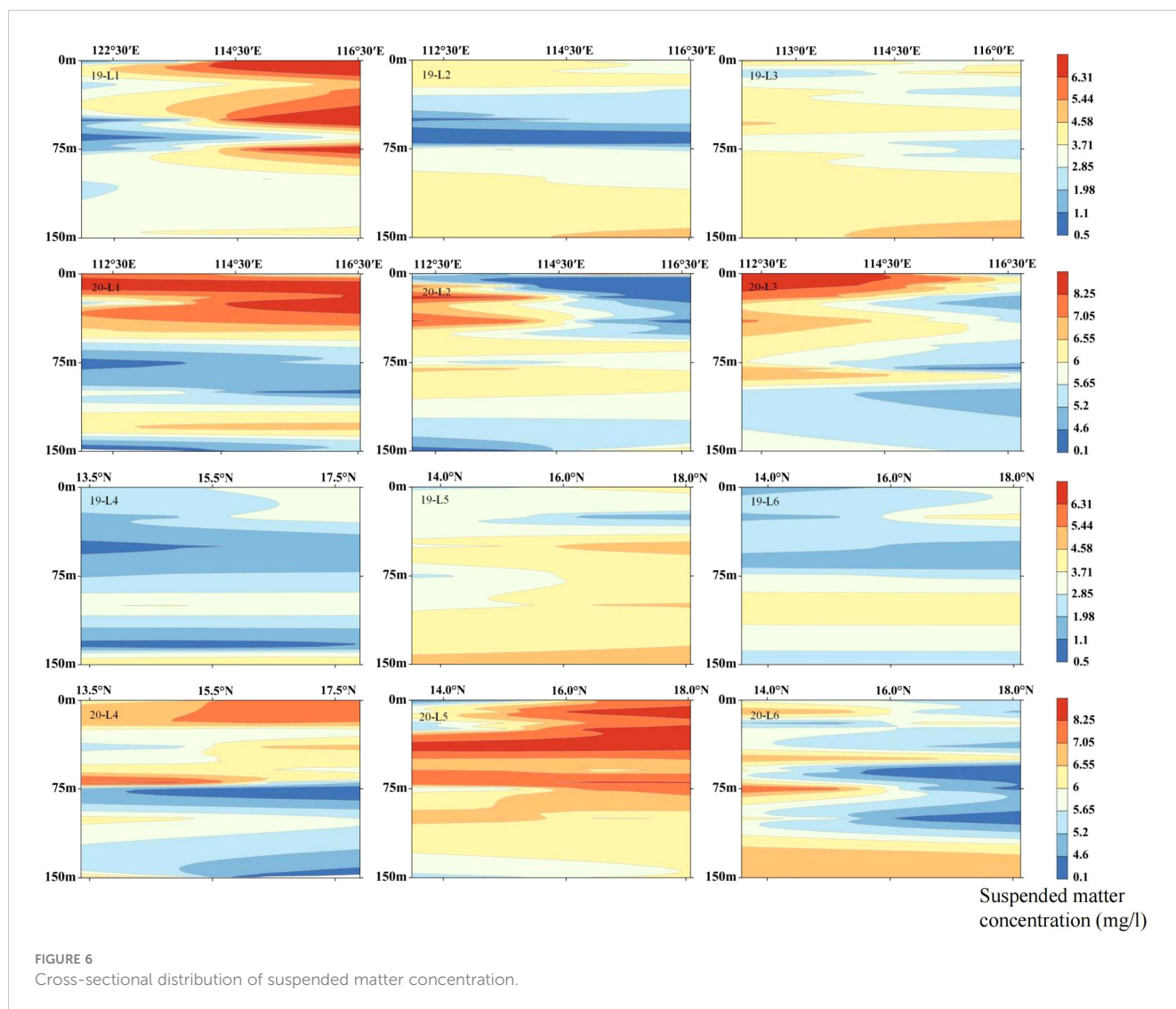
east overall. Likewise, the SMC in the 25-m, 50-m, and 100-m layers generally showed a similar decreasing trend from west to east. However, each layer has their own characteristics of horizontal distribution of SMC. High SMC value was found in the 25-m layer of the northeast area; the low values at 50 m is concentrated in the east area; low values in the 100-m layer is distributed in the northeast. In the 75-m layer, the SMC in the middle is substantially higher than its surroundings. The SMC in the 150 m layer was more uniform, except for the low values in the west.

3.4 Vertical distribution of suspended matter

To further look at the vertical distribution of SMC in the study area, we selected 6 representative cross-sections from each of the two surveys in 2019 and 2020 (Figures 1B and 6). In May 2019, the SMC at section L1 had lower values in the southwest than the northeast. The vertical distribution of higher SMC in the northeast was in a “three-peak” shape, with the amplitude of peaks step-wisely decreased with water depth. The lower SMC in the southwest was observed at 40–80m water depth, and its vertical distribution was in a “two-peak” shape. The SMC in the 100-m layer was nearly uniform across the L1 section. For section L2, the SMC decreased from 2.65–4.65 mgL^{-1} in 1–25 m layers to 0.25–1.00 mgL^{-1} in the 50–75m layers, and then increased to 2.8–3.1 mgL^{-1} in 75–100 m layers. The SMC at section L3 generally showed a “low-moderate-

low-moderate” pattern in the vertical direction. The SMC at 0–25 m layer was only 2.33 mgL^{-1} , in comparison with a higher 3.46 mgL^{-1} in 25–50 m layers. Downward from 50 m, the SMC decreased to 1.98–2.85 mgL^{-1} at 75 m in the northeast of this section and showed minor changes between 75 m and 150 m. SMC at Sections L4 and L6 is generally low, except for a relatively higher value 4.35 mgL^{-1} observed in the 100 m layer. In section L5, the vertical distribution of SMC was more uniform within the upper 100 m in the southwest; the SMC was higher in the 50–150 m layer after a low value appeared in the 25 m layer in the southeast.

In June 2020 when the summer monsoon prevails, SMC at section L1 showed a vertical distribution pattern of “high-low-medium” concentrations. SMC had values $> 6.55 \text{ mgL}^{-1}$ in the upper 50 m, $< 5.65 \text{ mgL}^{-1}$ in 50–100 m layers, and 5.65–6.55 mgL^{-1} in 100–150 m layers. For section L2, SMC in the upper 50 m was relatively higher in the southwest than in the northeast; below 50 m, SMC decreased with water depth. For section L3, the vertical distributions of both the high SMC in the southwest and low-SMC in the northeast section L3 showed a similar “three-finger”-like shape. Among them, the highest SMC values ($>7.05 \text{ mgL}^{-1}$) were found in the upper 25 m of the southwest area, in comparison with the low SMC in 100–150 m layers of the northeast area. Section L4 had a high SMC in the upper 25 m. Northwest areas had lower SMC in the 50 m layer but higher SMC in the 75 m than the southeast. At section L5, SMC generally decreased with water depth except for a higher value in the 25 m layer. Section L6 had higher SMC in northwest than the southeast.

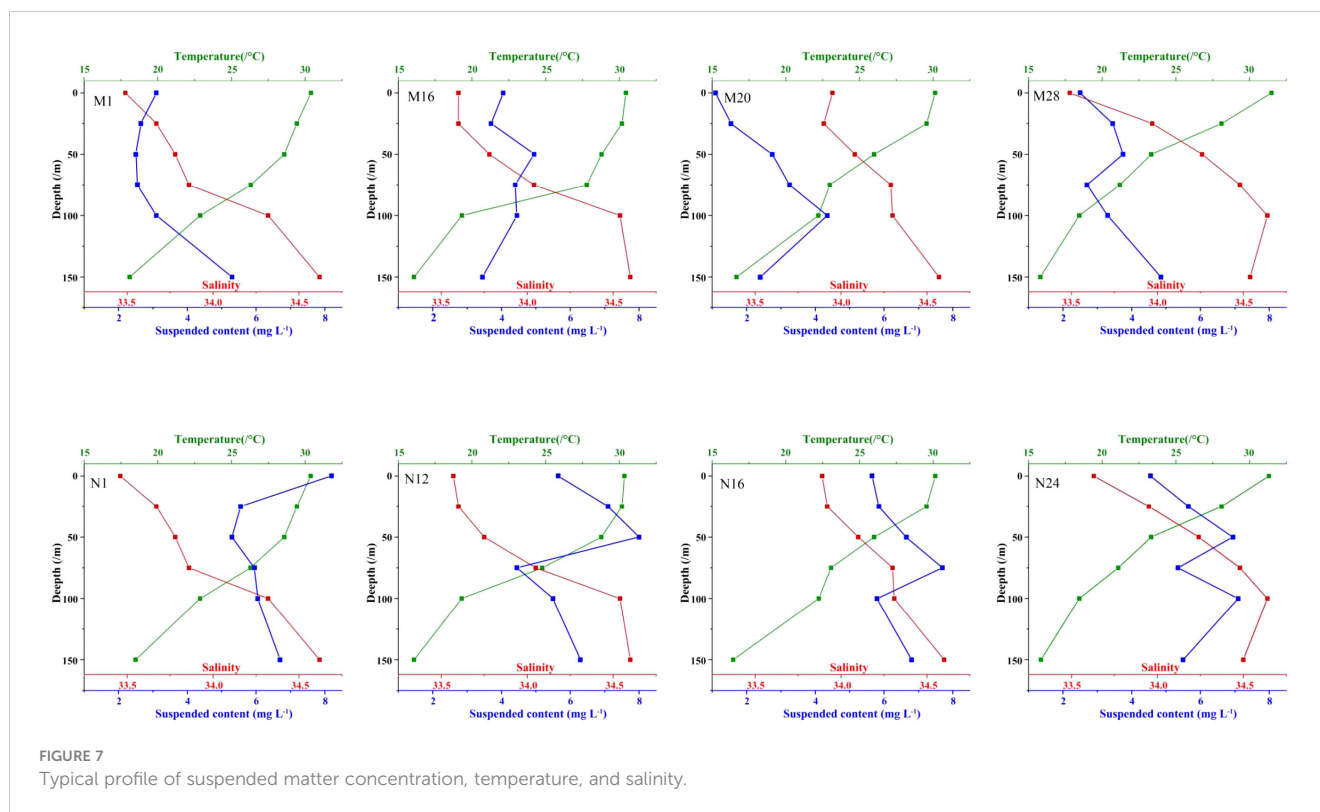


4 Discussion

4.1 Correlation between temperature, salinity, and SMC

In comparison with pre-monsoon (May 2019), the outbreak of summer monsoon in June 2020 led to higher temperature and SMC in all water layers, and greater discrepancies in SMC in deeper water layers with lower salinity in the ZGA. Previous studies have found that the SMC in the shallow water within the atoll increased faster owing to the combined influence of water depth and topography (Huang and Gao, 2012; Huang et al., 2022; Mao et al., 2005). We therefore argue that the seawater in the ZGA did not warm uniformly during the investigations in 2019 and 2020, due to the impacts of water depth and topography. We further selected four sampling stations in 2019 (M1, M16, M20, M28), and another 4 stations in 2020 (N1, N12, N16, N24) with complete sampling depth (150 m) for a detailed study in an attempt to reveal the relationship between SMC and temperature-salinity structure in seawater.

The results show that temperature and salinity structure in seawater at different depths had obvious correlations during the observations in May 2019 and June 2020 (Figure 7); the salinity increased while temperature decreased from the surface (1 m) to deep (150 m) water. The thermocline and halocline of seawater were situated at the 25 m, 75 m, and 100 m layers. In May 2019, seawater at the surface (1 m) and deep (150 m) layers had similar horizontal distribution of temperature and SMC, whereas the seawater at layers in between had different horizontal distributions of temperature and SMC. Whereas in June 2020, the horizontal distributions of temperature and SMC are nearly uniform across all water layers from the surface to the deep. This indicates that solar radiation may exert significant control on the variation in SMC. Despite the differences in the response of SMC to solar radiation in each layer, the locations of abrupt changes in SMC concurred with those of thermocline and halocline. This further indicates the changes in the temperature and salt structure led to different aggregation and distribution of plankton with or without preference for high temperature and salt, thus causing the changes in SMC. The planktonic organisms that affected the concentration



of the suspension layer included but were not limited to the diatoms and radiolarians identified in this study.

4.2 Influencing factors of SMC

4.2.1 Sources of suspended matter

Most of the ZGA area is dominated by underwater coral reef beaches with a total area of 8400 km², much larger than any other atolls in the South China Sea (Zuo et al., 2015). Since the Cambrian, nearly 1000-m-thick coral reefs have developed in this area (Arai, 2015; Huang et al., 2015). In the reef margin of the ZGA, dark sands, dark beaches, and coral reefs are uniformly distributed. Inside the lagoon, abundant species and large amounts of coral reefs are found, among which the reef-building stony corals are the dominant type. More than 30 types of reef-building stony corals are found in the northern and central areas only (Tong et al., 2015). Besides, a typical landscape of submarine plateau coral reef terrace leads to high biodiversity, biomass, and primary productivity (Leclerc and Feuillet, 2019). Together, these coral reef-sustained ecosystems provide abundant sources for the suspended matter, making the SMC in this area higher than that of most other deep ocean globally. SEM results showed that biogenic siliceous debris and plant fibers were the dominant components of the suspended matter in the study area, which accounts for 37.8% and 30.7%, respectively. Besides these two major components, authigenic minerals and modern anthropogenic materials respectively comprise 23.6% and 5.5%, while organic films are the least abundant, accounting for less than 1%. Together, these results indicate that the dominant sources of suspended matter in this

area are locally biogenic. In particular, high SMC was observed in the shallow water where the biological reefs were located, such as the locations of M23, M25, M31, M33, N19, N21, N27, and N29.

4.2.2 Topography

The elliptical ZGA is surrounded by deep waters >4000 m, becoming a “submarine plateau” with an average water depth of approximately 15–600 m (Chen et al., 2022; Xie, 1980). This topographic features lead to the overall transport of suspended matter in this area to the periphery centered on the Zhongsha Plateau, forming a convergence zone in the Zhongsha Trough in the western part of the study area. In addition, a submarine canyon the submarine canyon bridges the lagoon with the surrounding deep ocean, creating a “trumpet”-shaped mouth in the northeast part of the ZGA (Chen et al., 2022) where higher SMC (10mg L⁻¹) was found.

The dark sand edge of the ZGA protrudes, and the central part is a lagoon with scattered dark sands (Chen et al., 2022; Zhang et al., 2022), and many dark sands are distributed in the inner grooves and depressions with the accumulation of clean white coral sands and mesocosm debris. The edges of the dark sands are interrupted and disconnected, resulting in many independent individuals. The interrupted part becomes a natural waterway for suspended matter to enter and leave the lagoon, which accelerates the exchange of materials and energy inside and outside the lagoon and facilitates the appearance of high SMC, such as M16 and N12.

4.2.3 Ocean currents

During the transition of spring-summer monsoon (May 2019), the direction of the surface currents in the ZGA was generally easterly (Liu, 2010), with currents in the north flowing eastwards

and currents in the south flowing southeastwards (Guohong et al., 2005; Jilan, 2004; Su, 2004). This may be one of the primary controlling factors for the higher SMC observed in northwest (3.86 mgL^{-1}) than the southeast (3.12 mgL^{-1}) of the study area.

The outbreak of summer monsoon in 2020 resulted in a faster northeasterly current in the surface layer of the northwest of the ZGA and a northward current in the southwest, in comparison with an eastward current prevailing in other regions (Hu et al., 2000; Akhir, 2012; Wei et al., 2015). The fast-flowing current in the northwest brought considerable amounts of larger suspended particles to the west of ZGA and affected the seawater deeper than 50 m. These suspended particles led to a much higher mean SMC (6.27 mgL^{-1}) than that during the spring-summer monsoon transition in 2019 (3.26 mgL^{-1}). This monsoon-triggered current was also responsible for the horizontal SMC distribution pattern of “higher in the west and lower in the east”.

4.2.4 Wind field

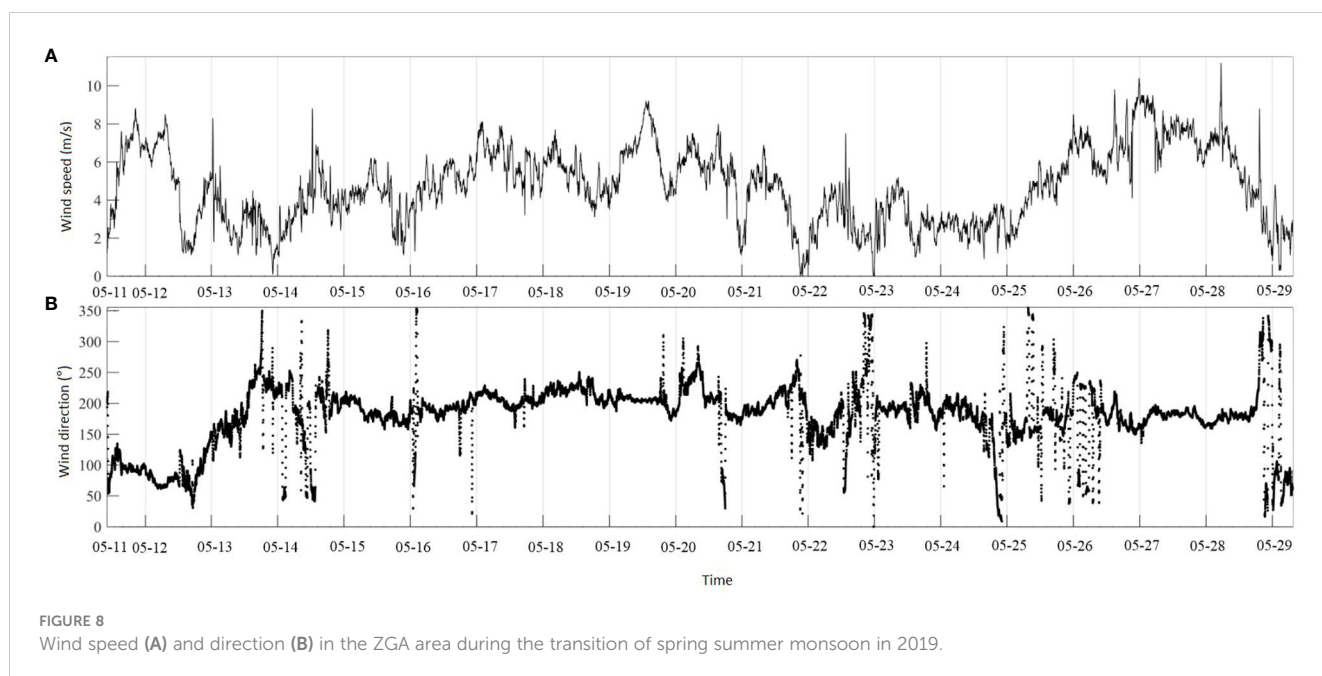
Wind direction and speed have been evidenced as a major control on the transport of suspended matter in ocean waters. The South China Sea is a monsoon-influenced area, and the wind speed during the spring and summer monsoon transition is characterized by small fluctuations, with northeasterly winds prevailing in most of the area; relatively higher wind speed of 3.5–5.0 m/s occurs in the north, (Wei et al., 2015). After the outbreak of the summer monsoon, the northeasterly winds shift to stable southwesterly winds originating from the tropics in most area of the ZGA (Cai et al., 2001; Mao et al., 2005). As shown in Figures 8 and 9, wind speed and direction changed greater during June 2020 than May 2019, indicating the dramatic influence of summer monsoon. Influenced by the summer monsoon, the suspended matter in this area is mainly transported northeasterly and southwesterly from the reef beach/dark sand at the perimeter of the terrace to the interior of the terrace, forming a clear zonation of higher SMC in the northwest and lower SMC in the southeast.

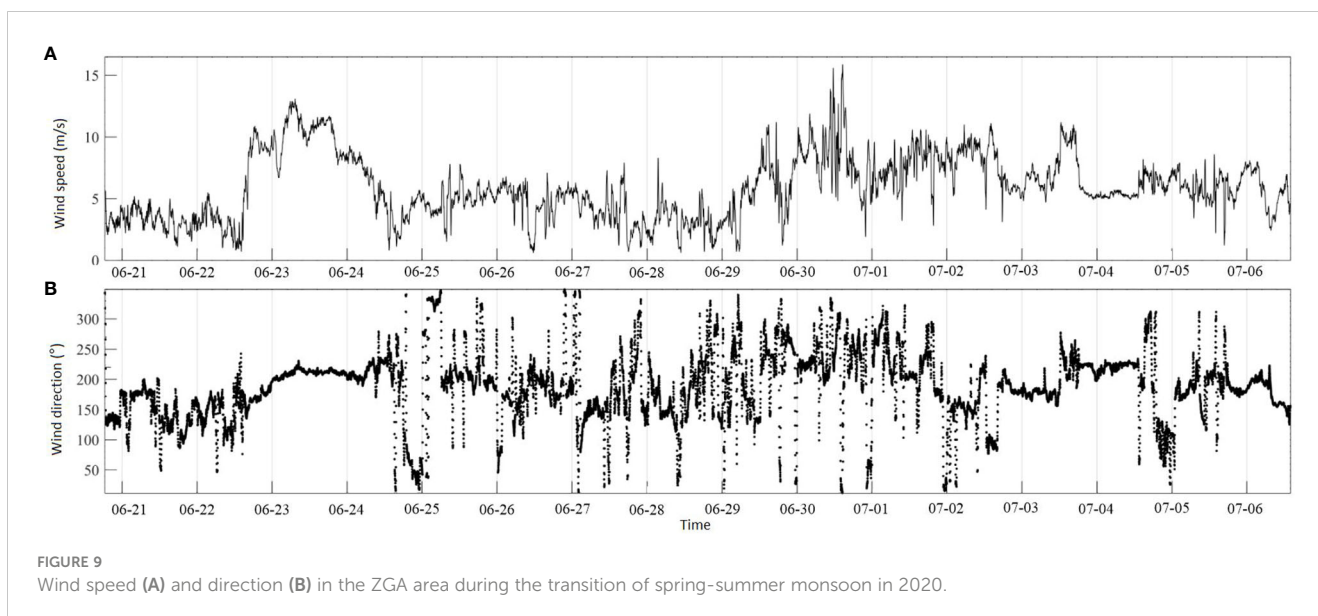
These winds drive the formation of wind-stress currents, together with the morphologic impacts (e.g. the existence of submarine canyon), determine the various directions of suspended mass transport from the Zhongsha Terrace to its surrounding waters. These transport directions include; 1) northwest to northeast as the main transport direction to the northern part of Zhongsha Trough in the north; 2) northwest to the west as the main transport direction to the middle part of Zhongsha Trough in the west; 3) southwest as the main transport direction to the southern part of Zhongsha Trough and Zhongsha South Ridge in the south; and 4) southeast as the main transport direction to the deep sea plain in the east. Suspended matter transported westward from the slope of the Zhongsha Plateau and eastward from the slope of the Xisha Rise meet in the waters of the Zhongsha Trough, forming a convergence zone (Wang et al., 2011). This may explain the high SMC in adjacent areas (M31, M32, M33, N27, N28, and N29).

5 Conclusion

Based on two field investigations conducted in May 2019 and June 2020, the composition, concentration, and spatial distribution of suspended matter was analyzed, and the following conclusions were drawn:

1. SMC decreased with water depth, with higher values observed in the west than the east, which correlates with the structures of seawater temperature and salinity. The outbreak of the summer monsoon in 2020 led to higher SMC than that before summer monsoon in 2019 and brought more larger suspended particles to the west.
2. High biodiversity, biomass, and primary productivity provide primary sources of suspended matter for this area. The richest type and quantity of suspended matter





in the ZGA are observed around the 25 m layer, which contains more than 20 types of materials.

3. Sources of suspended matter, topography, ocean currents, and wind fields were the main factors influencing the distribution of suspensions in the ZGA.

Our results provide a basic context for understanding the sources and transport of suspended matter in this area. Due to the limitation in spatial and temporal data coverage, we call for a systematic future investigation in the seasonal or intra-annual distribution of suspended matter in the ZGA and similar atolls globally, which is vital to decipher the biogeochemistry in these biodiversity systems.

Data availability statement

The original contributions presented in the study are included in the article/Supplementary Material, further inquiries can be directed to the corresponding author/s.

Author contributions

WY: Writing – original draft, Writing – review & editing, Conceptualization, Formal analysis, Software. JD: Investigation, Writing – original draft. DG: Conceptualization, Formal analysis, Funding acquisition, Visualization, Writing – original draft, Writing – review & editing. YW: Formal analysis, Methodology, Supervision, Writing – original draft. GX: Project administration, Resources, Writing – original draft. GW: Conceptualization, Writing – original draft. YS: Supervision, Validation, Writing – original draft. PL: Data curation, Investigation, Project administration, Writing – original draft. WC: Investigation, Software, Writing – original draft.

Funding

The author(s) declare financial support was received for the research, authorship, and/or publication of this article. This research was funded by the Special Project on Basic Resources Investigation (Grant No.2018FY100102) and the National Key Research and Development Program (Grant No. 2018YFC040800101).

Conflict of interest

The authors declare that the research was conducted in the absence of any commercial or financial relationships that could be construed as a potential conflict of interest.

Publisher's note

All claims expressed in this article are solely those of the authors and do not necessarily represent those of their affiliated organizations, or those of the publisher, the editors and the reviewers. Any product that may be evaluated in this article, or claim that may be made by its manufacturer, is not guaranteed or endorsed by the publisher.

Supplementary material

The Supplementary Material for this article can be found online at: <https://www.frontiersin.org/articles/10.3389/fmars.2024.1268294/full#supplementary-material>

References

- Akhir, M. F. M. (2012). Surface circulation and temperature distribution of southern South China Sea from global ocean model (OCCAM). *Sains Malaysiana* 41 (6), 701–714. doi: 10.2183/pjab.88.266
- Arai, T. (2015). Diversity and conservation of coral reef fishes in the Malaysian South China Sea. *Rev. Fish Biol. Fisheries* 25, 85–101. doi: 10.1007/s11160-014-9371-9
- Bubnova, E. S., Kapustina, M. V., Krechik, V. A., and Sivkov, V. V. (2020). Suspended matter distribution in the surface layer of the East Equatorial Atlantic. *Oceanology* 60, 228–235. doi: 10.1134/S000143702001004X
- Cai, S. Q., Su, J. L., and Gan, Z. J. (2001). Response of South China Sea upper circulation to monsoon transition. *J. Trop. Oceanogr.* 20 (3), 52–60.
- Chen, J. F., Zheng, L. F., Chen, R. H., Zheng, Y. L., Chen, W. B., Wiesner, M. G., et al. (1998). Fluxes and constituents of particulate matter in the South China Sea in comparison with sediment accumulation rates. *Acta Sedimentol. Sin.* 03, 14–19.
- Chen, J. J., Zhang, J. W., Liu, S. Q., Chen, W. L., Qin, Y. Y., and Wu, S. G. (2022). Grain size distribution pattern of surface sediments and its implications for transportation trend: A case from the waters off Zhongsha Islands, the South China Sea. *Mar. Geol. Quaternary Geol.* 42 (02), 15–27.
- Chong, G. P., Wei, Y. U., Yang, Y., and Dan, X. H. (2011). An improved method for evaluating the seasonal variability of total suspended sediment flux field in the Yellow and East China Seas. *Int. J. Sediment Res.* 26 (1), 1–14. doi: 10.1016/S1001-6279(11)60071-1
- Guo, Z. G., Yang, Z. S., Lei, K., Gao, L., and Yan-Hui, Q. U. (2001). The distribution and composition of suspended matters and their influencing factors in the central-southern area of Okinawa Trough and its adjacent shelf sea. *Acta Oceanol. Sin.* 01, 66–72+143.
- Guohong, F., Susanto, D., Soesilo, I., Zheng, Q. A., Fangli, Q., and Zexun, W. (2005). A note on the South China Sea shallow interoccean circulation. *Adv. Atmos. Sci.* 22, 946–954. doi: 10.1007/BF02918693
- Hu, J. Y., Karamura, H., and Hong, H. H. (2000). A review on the currents in the South China Sea: Seasonal circulation, South China Sea Warm Current and Kuroshio intrusion. *J. Oceanogr.* 56 (6), 607–624. doi: 10.1023/A:1011117531252
- Huang, X., Betzler, C., Wu, S., Bernhardt, A., Eagles, G., Han, X., et al. (2020). First documentation of seismic stratigraphy and depositional signatures of Zhongsha atoll (Macclesfield Bank), South China Sea. *Mar. Pet. Geol.* 117, 104349. doi: 10.1016/j.marpetgeo.2020.104349
- Huang, L., and Gao, H. F. (2012). Analyses on temperature and salinity distributions in Zhongsha Islands waters during spring to summer monsoon Transition. *Geol. Res. South China Sea* 1, 49–56.
- Huang, H., He, E., Qiu, X., Guo, X., Fan, J., and Zhang, X. (2020). Insights about the structure and development of Zhongsha Bank in the South China Sea from integrated geophysical modelling. *Int. Geol. Rev.* 62 (7-8), 1070–1080. doi: 10.1080/00206814.2019.1653798
- Huang, D., Licuanan, W. Y., Hoeksema, B. W., Chen, A. C.L., Ang, P. O., Huang, H., et al. (2015). Extraordinary diversity of reef corals in the South China Sea. *Mar. Biodivers.* 45, 157–168. doi: 10.1007/s12526-014-0236-1
- Huang, C., Wu, N. Y., Wu, X., Liu, S. Q., Zhang, J. W., Xu, C., et al. (2022). Temporal-spatial variation characteristics and the controlling factors of temperature and salinity structure in Zhongsha Islands sea area of the South China Sea. *Mar. Geol. Quaternary Geol.* 42 (2), 1–14. doi: 10.16562/j.cnki.0256-1492.2021111301
- Jilan, S. (2004). Overview of the South China Sea circulation and its influence on the coastal physical oceanography outside the Pearl River Estuary. *Cont. Shelf Res.* 24 (16), 1745–1760. doi: 10.1016/j.csr.2004.06.005
- Leclerc, F., and Feuillet, N. (2019). Quaternary coral reef complexes as powerful markers of long-term subsidence related to deep processes at subduction zones: Insights from Les Saintes (Guadeloupe, French West Indies). *Geosphere* 15 (4), 983–1007. doi: 10.1130/GES02069.1
- Liu, Y. (2010). *Study on the structures and the kinetics characteristics for the subsurface and intermediate water masses in the South China Sea* (Qingdao: Ocean University of China).
- Liu, S., Pan, Y. F., Li, H. X., Lin, L., Hou, R., Yuan, Z., et al. (2022). Microplastic pollution in the surface seawater in Zhongsha Atoll, South China Sea. *Sci. Total Environ.* 822, 153604. doi: 10.1016/j.scitotenv.2022.153604
- Manik, H. M., and Firdaus, R. (2021). Quantifying suspended sediment using acoustic doppler current profiler in Tidung Island seawaters. *Pertanika J. Sci. Technol.* 29 (1), 363–385. doi: 10.47836/pjst.29.1.21
- Mao, Q. W., Wang, W. Q., and Qi, Y. Q. (2005). Analyses on temperature and salinity distributions in Nansha Islands waters during spring to summer monsoon transition. *J. Trop. Oceanogr.* 24 (1), 28–36.
- Milliman, J. D., and Syvitski, J. P. (1992). Geomorphic/tectonic control of sediment discharge to the ocean: the importance of small mountainous rivers. *J. Geol.* 100 (5), 525–544. doi: 10.1086/629606
- Nittrouer, C. A., DeMaster, D. J., Kuehl, S. A., Figueiredo, A. G. Jr., Sternberg, R. W., Faria, L. E. C., et al. (2021). Amazon sediment transport and accumulation along the continuum of mixed fluvial and marine processes. *Annu. Rev. Mar. Sci.* 13, 501–536. doi: 10.1146/annurev-marine-010816-060457
- Quanshu, Y., Xuefa, S., and Kunshan, W. (2007). Mineral provinces and material provenance of the surficial sediments near the Zhongsha Islands in the South China Sea. *Acta Oceanol. Sin.* 1), 66–76. doi: 10.1109/UT.2007.370822
- Su, J. L. (2004). Overview of the South China sea circulation and its influence on the coastal physical oceanography outside the Pearl River Estuary. *Cont. Shelf Res.* 24 (16), 1745–1760. doi: 10.1016/j.csr.2004.06.005
- Sun, J., Hamel, J. F., and Mercier, A. (2018). Influence of flow on locomotion, feeding behaviour and spatial distribution of a suspension-feeding sea cucumber. *J. Exp. Biol.* 221 (20), jeb189597.
- Tong, F., Chen, P. M., Qin, C. X., and Li, X. G. (2015). Species diversity and scleractinian corals distribution at two shoals of Zhongsha Islands, South China Sea. *J. Appl. Oceanogr.* 34 (04), 535–541.
- Wang, N. (2014). *Sedimentary dynamics process and topographic evolution in the modern Yellow River mouth*. PhD Thesis. Shandong, China: Ocean University of China.
- Wang, H., Jia, Y., Ji, C., Jiang, W., and Bian, C. (2022). Internal tide-induced turbulent mixing and suspended sediment transport at the bottom boundary layer of the South China Sea slope. *J. Mar. Syst.* 230, 103723. doi: 10.1016/j.jmarsys.2022.103723
- Wang, Y. Z., Ju, X., Du, J., Liu, Z. J., Wang, D. W., Zhou, R. S., et al. (2022). Characteristics of the temperature and salinity distribution in adjacent sea areas of Zhongsha Islands during spring-summer transition period. *Adv. Mar. Sci.* 40 (3), 408–422.
- Wang, G. H., Xie, S. P., Qu, T. D., and Huang, R. X. (2011). Deep South China seacirculation. *Geophys. Res. Lett.* 38 (5), L05601.
- Wei, Z., Lian, Z., and Yang, Y. (2015). Development of an ocean current forecast system for the South China Sea. *Aquat. Proc.* 3, 157–164. doi: 10.1016/j.aqpro.2015.02.206
- Xie, Y. X. (1980). Underwater topography of Zhongsha Islands. *Mar. Sci. Technol. Data* 01, 39–45.
- Zhang, Y., Liu, S., Zhang, L., Zhou, Y., Liang, J., Lu, J. A., et al. (2022). Application of singularity theory to the distribution of heavy metals in surface sediments of the Zhongsha Islands. *J. Mar. Sci. Eng.* 10 (11), 1697. doi: 10.3390/jmse10111697
- Zuo, X., Su, F., Wu, W., Chen, Z. K., and Shi, W. (2015). Spatial and temporal variability of thermal stress to China's coral reefs in South China Sea. *Chin. Geogr. Sci.* 25, 159–173. doi: 10.1007/s11769-015-0741-6